Postmetallization "Passivated Edge Technology" for Separated Silicon Solar Cells

Puzant Baliozian, Mohammad Al-Akash, Elmar Lohmüller, Armin Richter, Tobias Fellmeth, Anna Münzer, Nico Wöhrle, Pierre Saint-Cast, Hannah Stolzenburg, Alma Spribille, and Ralf Preu

***Abstract*—This article introduces a postmetallization "passivated edge technology" (PET) treatment for separated silicon solar cells consisting of aluminum oxide deposition with subsequent annealing. We present our work on bifacial shingle solar cells that are based on the passivated emitter and rear cell concept. To separate the shingle devices after metallization and firing, we use either a conventional laser scribing mechanical cleaving (LSMC) process or a thermal laser separation (TLS) process. Both separation processes show similar pseudo fill factor (pFF) drops of $-1.2\%_{\mathrm{abs}}$ from the host wafer to the separated state. The *pFF* of the TLS-separated cells increases by up to $+0.7\%_{\mathrm{abs}}$ from the as-separated state after PET treatment due to edge passivation, while the *pFF* of LSMC-separated cells increases by up to $+0.3\%_{\mathrm{abs}}$. On cell level, the combination of TLS and PET allows for a designated area output power density of $p_{\mathrm{out}} = 23.5$ mW/cm², taking into account an additional 10% rear side irradiance.**

***Index Terms*—ALD, aluminum oxide, bifacial PERC, passivated edge technology, postmetallization, shingle solar cells, thermal laser separation (TLS).**

I. Introduction

THE REVIVAL of the shingling interconnection approach of solar cells [1] is an option to obtain higher photovoltaic module output power densities p_{out}. Shingling of solar cells is done by interconnecting the rear busbar of a cell to the front busbar of a neighboring one. The overlap and the interconnection of the busbars lead to: (i) the removal of cell spacing and therefore to an increase of active cell area within the module, (ii) the decrease of shading losses due to the absence of visible busbars and interconnectors, and (iii) the decrease of electrical resistance losses on the interconnection level. Shingling solar cells have first been used for niche applications such as satellite devices [2], electronic devices [3], and electrical vehicle prototypes [4]. The potential shown by the shingling approach leads to the recent increase in interest not only shown in publications [5]–[8] and patents [9]–[11], but also in already existing commercially available shingle modules [12], [13].

Similar to half-size cells [14], shingle cells are usually separated from metallized and fired host wafers. The separation process leads to a decrease in solar cell efficiency due to edge recombination induced by the separation [15]. Edge recombination becomes even more significant for small-sized cells with higher perimeter-to-area ratios, leading to losses mainly in fill factor *FF* (initially caused by losses in pseudo fill factor *pFF*) in addition to losses in open-circuit voltage V_{OC}.

Edge recombination can be reduced by: (i) the depletion of charge carriers of a kind from the edge and/or (ii) the reduction of density of traps at the edge. As review of potential methods for edge passivation, we find that some previously investigated methods to reduce edge recombination of solar cells consist of introducing an emitter window commonly created by the use of diffusion barriers [16], [17]. The emitter window cuts off the emitter conduction towards the edge, thus reducing the support of minority charge carriers tremendously. Having the same aim, the removal of the emitter by creating passivated isolation trenches is proposed as another approach [18]. In this method, the trenches are formed by ablating the emitter, followed by wet-chemical etching, and finally, passivating the trenches by thermally grown silicon dioxide (SiO_2) or polysilicon. In Ref. [19], a strong doping at the separation path is suggested to create a repulsion of carriers from the edge by a surface field effect. It has also been reported that treating the edge wet-chemically allows the growth of SiO_2 on the edge, which shows a passivation effect [20]. In Ref. [21], the surface passivation of two sawed slits tens of micrometers far from the cell active area is achieved by the deposition of aluminum oxide, capped by silicon nitride, and silicon oxide layers. The process is done after partially damage etching the slit surfaces.

However, fabricating such cells requires several additional premetallization process steps [22] or postmetallization chemical etching processes, which make the implementation on industrial fabrication scale challenging. Simulation results confirm the positive effect of passivated edges on shingle cells by reducing the effective surface recombination velocity at the edge, $S_{\mathrm{eff,edge}}$ [23], [24]. Nevertheless, no potentially industrial feasible process is found in literature.

This article introduces the concept of postmetallization "passivated edge technology" (PET). The PET is demonstrated on bifacial *p*-type silicon shingled passivated edge, emitter, and rear (*p*SPEER) solar cells, which have been initially reported without

Manuscript received September 2, 2019; revised November 9, 2019; accepted December 6, 2019. This work was supported by the German Federal Ministry for Economic Affairs and Energy within the research project "PV-BAT400" under Contract 0324145. *(Corresponding author: Puzant Baliozian.)*

The authors are with the Fraunhofer Institute for Solar Energy Systems ISE, 79110 Freiburg, Germany (e-mail: puzant.baliozian@ise.fraunhofer.de; mohammad.al-akash@ise.fraunhofer.de; elmar.lohmueller@ise.fraunhofer.de; armin.richter@ise.fraunhofer.de; tobias.fellmeth@ise.fraunhofer.de; anna.muenzer@ise.fraunhofer.de; nico.woehrle@ise.fraunhofer.de; pierre.saint-cast@ise.fraunhofer.de; hannah.stolzenburg@ise.fraunhofer.de; alma.spribille@ise.fraunhofer.de; ralf.preu@ise.fraunhofer.de).

Color versions of one or more of the figures in this article are available online at http://ieeexplore.ieee.org.

Digital Object Identifier 10.1109/JPHOTOV.2019.2959946

PET in Ref. [25]. The bifacial *p*SPEER cell concept is based on the passivated emitter and rear cell (PERC) [26] architecture, where an additional laser-assisted separation process is applied to obtain the cell stripes. The separation processes investigated in this article are conventional laser scribing and mechanical cleaving (LSMC) and thermal laser separation (TLS) [27], [28]. The effect of the separation processes and the edge passivation are discussed together with the first solar cell results.

II. Passivated Edge Technology and Cell Characterization

A. *pSPEER^{PET} Solar Cell Concept*

The separation process leads to an increase of edge recombination, especially when the emitter extends to the separated edges; see Fig. 1(a) for a schematic cross section of the *p*SPEER cell. The cells only have a natively grown SiO_2 layer at the edge. For that reason, an additional postmetallization/separation PET aims to decrease $S_{\mathrm{eff,edge}}$ by coating the edges with an intended dielectric passivation layer. The "*p*SPEER$^{\mathrm{PET}}$" solar cell is obtained after edge passivation by the PET; see Fig. 1(b). In this article, the PET consists of two steps: a postmetallization/separation deposition of an aluminum oxide (AlO_X) layer and a postdeposition annealing (PDA) for the activation of the deposited AlO_X passivation layer. Thermal atomic layer deposition (ALD) is used for the AlO_X deposition. This has several advantages: (i) ALD is known for a very conformal deposition, e.g., the wafer edge is well coated after the process; (ii) AlO_X can provide an excellent surface passivation because it combines enhanced chemical passivation with a strong field effect passivation induced by a high amount of fixed negative charges [29]; (iii) it is transparent for very thin films of thicknesses d ranging between 5 nm $\leq d \leq$ 15 nm [30]. OPTOS simulations done on module level confirm that such thin AlO_X layers deposited on the front and rear surfaces of the cells do not induce optical losses; (iv) the passivation effect of thermal ALD-deposited AlO_X is known to be activated at low annealing temperatures $T_{\mathrm{ann}} < 225$ °C [31], [32]. The latter hinders thermally induced metal contact degradation which has been reported [33].

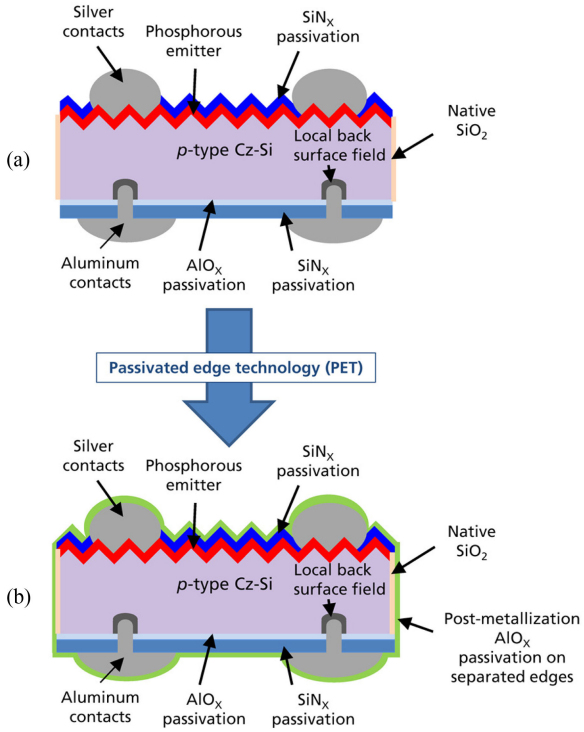

Fig. 1. (a) Schematic cross section of a bifacial *p*SPEER solar cell. The structure is similar to the bifacial PERC concept with additional separated edges covered by native SiO_2. (b) After PET, the *p*SPEER$^{\mathrm{PET}}$ solar cell has an additional postmetallization dielectric passivation layer (i.e., AlO_X) all over the cell and, most importantly, at the separated edges (green layer). In both figures (a) and (b), the external contacts (rear-side silver busbars) are not shown.

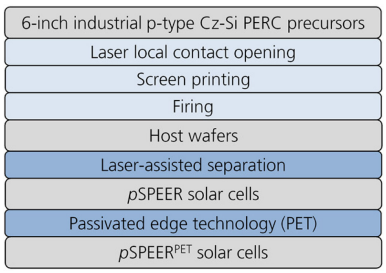

Fig. 2. Process flow of the *p*SPEER$^{\mathrm{PET}}$ solar cell's fabrication from industrial-passivated 6-inch *p*-type Cz-Si:Ga PERC precursors.

B. *Solar Cell Fabrication*

Industrial 6-inch gallium-doped Czochralski-grown silicon (Cz-Si:Ga) PERC precursors are used for the fabrication of the *p*SPEER and *p*SPEER$^{\mathrm{PET}}$ cells investigated in this article. Fig. 2 shows the corresponding fabrication process. The precursors' base resistivity ranges between 0.3 Ω cm $\leq \rho_B \leq$ 0.9 Ω cm. The front phosphorous-doped emitter is passivated by a silicon nitride (SiN_X) layer; the rear silicon base is passivated by a layer stack consisting of AlO_X capped by SiN_X. The precursors are optimized for monofacial use, which explains the yellowish color of the rear side; see Fig. 3(a). The fabrication process performed in this article starts from the laser contact openings. The rear side silver busbars (external contacts) are screen printed first. Next, the rear-side aluminum contact grid and the front-side silver contact grid are printed. Contact firing is then performed in an industrial fast firing oven. The printed metallization layouts are designed to obtain six shingle devices from one host wafer [each exhibiting the dimensions 22 mm × 148 mm; see Fig. 3(b)]. Finally, six individual shingle cells are obtained after laser-assisted separation as shown in Fig. 3(c).

The performed separation processes in this article are (i) conventional LSMC and (ii) TLS, both implemented by using the *microDICE* tool from *3D-Micromac* [34]. The following items describe the processes:

1) LSMC is done by a nanosecond infrared pulsed laser that scribes along the entire separation path and ablates up to one-third of the substrate's thickness. Consequently, the samples are manually and mechanically cleaved.
2) TLS is performed by creating an initial scribe by means of the same pulsed laser used in the LSMC process to start a crack of length between 0.5 mm $\leq l \leq$ 1 mm. For the

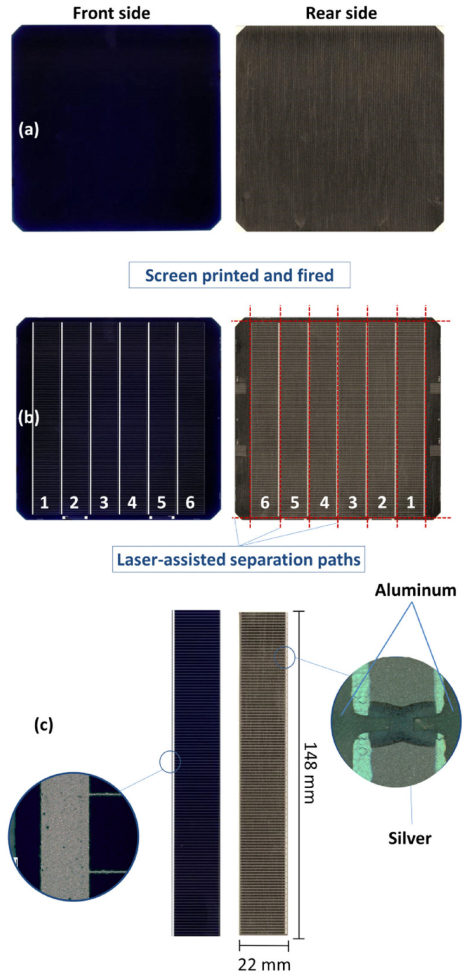

Fig. 3. Scanned images of the front side and rear side of (a) an industrial 6-inch PERC precursor, and (b) a metallized host wafer with the metallization layouts from which six cells can be separated. (c) pSPEER cells after laser-assisted separation with the dimensions 22 mm × 148 mm. Microscope images show the metallization on the front and rear sides. The figure is adapted from Ref. [35].

cleave process, an infrared continuous wave laser in combination with a simultaneous water/air cooling jet is used to thermally induce a compressive stress and consequent tensile stress along the separation path. This leads to the cleavage of the substrate.

Planar view scanning electron microscope (SEM) images of exemplary cell edges for LSMC and TLS processed samples are shown in Fig. 4(a) and (b), respectively. The edge obtained by LSMC has a rough laser-scribed region which is about one-third of its thickness. The mechanically cleaved part of the edge is rather smooth. In contrast, the cell edge obtained by the TLS process shows an entirely smooth surface.

C. SunsV_{OC} and Current–Voltage Characterization

In this article, SunsV_{OC} measurements [36], [37] are performed to characterize the effect of the separation and passivation processes. By this method, the effect of edge recombination on the solar cell performance is independent of possible changes

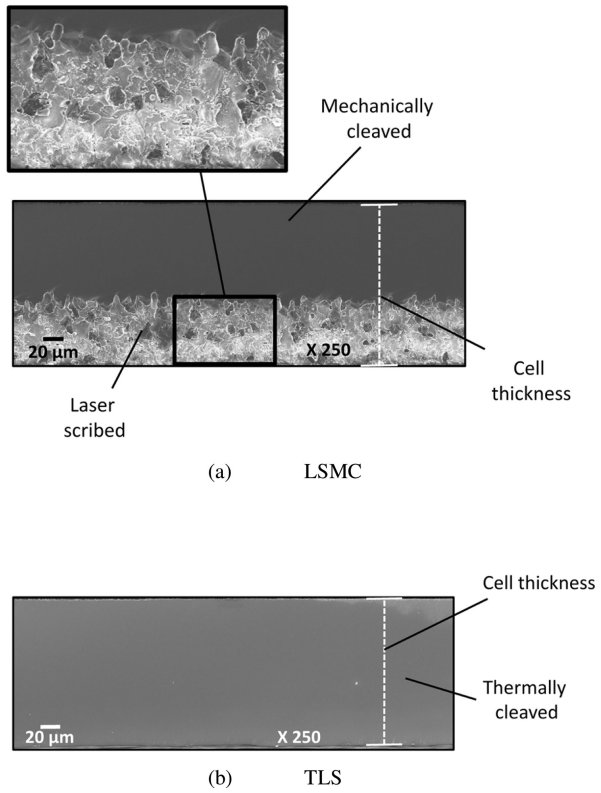

Fig. 4. SEM images of (a) cell edge separated by an LSMC process. The scribe-laser-induced roughness dominates around one-third of the thickness. (b) Cell edge separated by TLS with substantially smoother edges due to the complete thermal cleave as a result of the process.

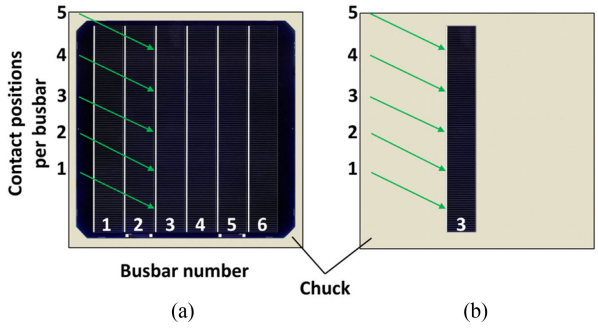

Fig. 5. (a) Schematic of contacting positions during the SunsV_{OC} measurement of the host wafer before separation. Five positions are contacted per busbar (here busbar 3 is taken as an example). (b) Contacting of a shingle cell on the busbar at the same five positions. The separated cell is placed on the chuck at the position where it was positioned prior to its separation.

in series resistance r_S. From the measurements, pFF and V_{OC} values at an illumination intensity of 1000 W/m^2 are extracted. In order to exclude effects of local inhomogeneity (either from the host wafers or from the SunsV_{OC} measurement setup), each host wafer is measured at five different positions on each busbar; see Fig. 5(a). Separated cells are then placed at the same position on the SunsV_{OC} chuck as measured prior to separation within the host wafer; see Fig. 5(b). After each additional process step performed on the cell, it is contacted and measured in an

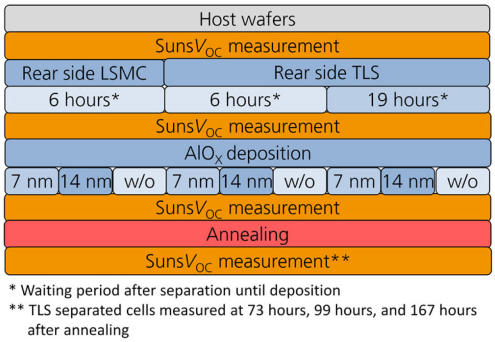

Fig. 6 Experimental process and characterization steps to investigate the effect of PET on separated cells.

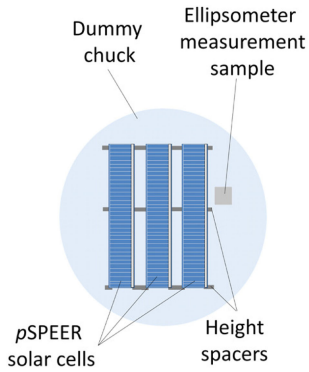

Fig. 7. Top view sketch of three shingle cells, an ellipsometer measurement sample, and the spacers during the PET deposition process in the *FlexAL*. The cells are placed with the front side facing up. The deposition on the front and rear sides is intended by spacers.

identical way. A reference cell not undergoing any process steps is measured continuously throughout the experiments to track the reproducibility of the SunsV_{OC} measurement.

The illuminated current–voltage (IV) measurement is done at standard test conditions on each side separately using an industrial cell tester calibrated by a reference *p*SPEER cell measured at Fraunhofer ISE CalLab PV Cells. During the IV-testing procedure, the cells are placed on a black, nonconducting background, which ensures negligible reflection well below 5% over the relevant spectrum. The contacting is performed at the front- and rear-side busbars by pin arrays.

III. Edge Passivation

A. Experimental Plan for PET on Cells

The aim of this experiment is to observe the effect of the separation processes from host wafer to separated state by using SunsV_{OC} measurements; see the experimental process flow in Fig. 6. In addition, the effect of the AlO_X deposition and subsequent annealing on cells is examined. LSMC is done 6 h before AlO_X deposition. The TLS-diced host wafers are separated also 6 h prior to the AlO_X deposition, while another group is TLS-diced 19 h prior to the AlO_X deposition. The different separation dates are to investigate the influence of the waiting time between separation and deposition. In air at room temperature, native SiO_2 growth occurs on exposed silicon [38]. Due to the logarithmic growth of SiO_2 as a function of exposure time to air, similar layer thicknesses are expected for both waiting times in this article.

The AlO_X deposition process is performed in a *FlexAL* reactor of *Oxford Instruments* [39] using trimethylaluminum and water vapor as precursors. Two deposited AlO_X layer thicknesses are investigated: $d_1 = 7$ nm and $d_2 = 14$ nm, as measured with spectroscopic ellipsometry on a planar silicon process control sample. Three to four separated cells have been processed in each deposition run (see Fig. 7). Height spacers are used to ensure a deposition on the rear side as well.

SunsV_{OC} measurements before and after deposition are completed by contacting at five measurement positions per busbar. Postdeposition hotplate annealing (PDA) is performed at temperature $T_{\mathrm{ann}} < 225$ °C. Control cells (without deposition) from each separation process are kept and are not coated with AlO_X to observe the effect of the annealing process on the non-coated cells. SunsV_{OC} measurements are then done after PDA. To investigate the stability of the passivation effect, TLS-separated cells are measured again after 73, 99, and 167 h.

To understand the effect of the deposition and annealing processes and estimate the effective surface recombination velocity S_{eff}, a symmetrical lifetime sample (*n*-type float-zone silicon, $\rho_{\mathrm{B}} \approx 1\ \Omega$ cm, wafer thickness $W \approx 200\ \mu$m) is coated with $d_1 = 7$ nm AlO_X layer.

Quasi-steady-state photoconductance (QSSPC) measurements [40] are performed to obtain the minority carrier lifetime τ_{eff} dependency on the excess carrier density Δn at the following states: (i) as-deposited and (ii) annealed. S_{eff} is then approximated by using [41]

$$1 \,/\, \tau_{\mathrm{eff}} = (1 \,/\, \tau_{\mathrm{bulk}}) + (2S_{\mathrm{eff}} \,/\, W)\,. \tag{1}$$

Noting that τ_{bulk} is the intrinsic bulk lifetime and τ_{eff} is extracted at $\Delta n = 10^{15}$ cm^{-3}.

IV. Results and Discussion

A. Effect on Charge Carrier Lifetime

The QSSPC measurement of the lifetime sample in Fig. 8 shows the injection-dependent lifetime obtained by means of QSSPC for the as-deposited and annealed states. After annealing, $\tau_{\mathrm{eff}} = 432\ \mu$s at $\Delta n = 10^{15}$ cm^{-3} is measured.

Using (1), $S_{\mathrm{eff}} = 22$ cm/s is obtained, showing the possibility of attaining low S_{eff} values by the current deposition/annealing method. Note that the planar S_{eff} is not necessarily equal to that of the edge due to different surface and geometrical conditions.

B. SunsV_{OC} Results

1) Effect of PET: From the SunsV_{OC} measurements, we extract V_{OC} values at an illumination intensity of 1000 W/m² and the *pFF*. The host wafers attain mean $V_{\mathrm{OC}} = 669$ mV. The changes in V_{OC} throughout the process steps are minor, with a maximum variation of $\Delta V_{\mathrm{OC}} = \pm\, 2$ mV. This small impact on V_{OC} is in agreement with simulation results for similar sample types and V_{OC} levels [23], [42].

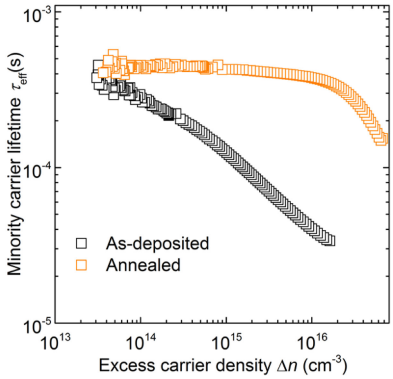

Fig. 8. QSSPC measurement of the minority carrier lifetime τ_{eff} dependent on excess carrier density Δn for the symmetrical n-type float-zone silicon lifetime samples. After annealing, the sample attains $\tau_{\mathrm{eff}} = 432\ \mu$m extracted at $\Delta n = 10^{15}$ cm^{-3} (≈ 1000 W/m^2 illumination level).

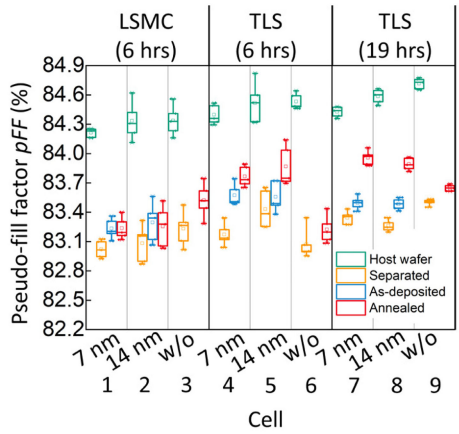

Fig. 9. SunsV_{OC} measurement results of host wafers, after separation, as-deposited, and annealed. Control cells without deposition are also measured before and after annealing. The hours on the top of the plot indicate the approximate time gap between separation and deposition.

Hence, we focus on the *pFF* data which are shown in Fig. 9. The values are given for the four different sample states: (i) host wafer, (ii) separated, (iii) as-deposited, and (iv) annealed. They are divided into the different separation groups and AlO_X layer thicknesses. The results are discussed considering the state-to-state changes.

To start with, LSMC and TLS separation processes lead to a decrease in *pFF* ($\Delta pFF = -1.2\%_{\mathrm{abs}}$) from the host wafer to the separated state due to similar edge recombination effects.

Noticeably, the introduction of the AlO_X layer with thickness d_1 or d_2 leads to an improved edge passivation and thus to a gain in *pFF*. The deposition on TLS-separated cells leads to the highest increase from separated to as-deposited state reaching $\Delta pFF = +0.4\%_{\mathrm{abs}}$.

After annealing, the TLS-separated and coated cells show the highest increase, $\Delta pFF = +0.4\%_{\mathrm{abs}}$ from as-deposited to annealed states. Such an increase after PDA is due to the activation of the passivation layers that coat the smooth edge surface. Annealing of control cells without deposition leads to an enhanced *pFF*. This is probably due to the grown SiO_2 on the edges, which is allowed by the absence of the AlO_X coating.

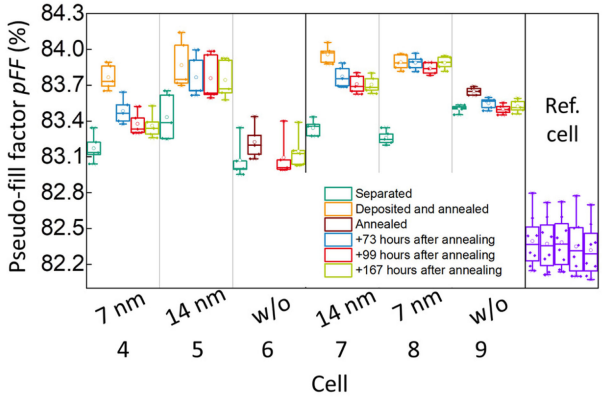

Fig. 10. *pFF* values attained by SunsV_{OC} measurements of TLS-separated cells before and after PET. The same cells are measured 73, 99, and 167 h after PET. Measurements of TLS-separated cells that are annealed without undergoing deposition are included. The reproducibility of the measurement is verified by a reference cell.

As an assessment of PET, the TLS-separated cells show higher *pFF* gains than the LSMC-separated ones when both PET process steps (deposition and PDA) are completed. The deposition on a smooth surface with reduced defects obtained by TLS and the activation of the deposited passivation layer lead to the highest *pFF* increase of $+0.7\%_{\mathrm{abs}}$ and the highest measured *pFF* values. TLS-separated cells regain up to $50\%_{\mathrm{rel}}$ of their initial *pFF* loss due to the separation process (observed for both deposition thicknesses and separation groups), and control cells that are not coated and are only annealed do not show such a regain. LSMC-separated cells regain around $16\%_{\mathrm{rel}}$ after PET. This shows that PET leads to edge passivation for both separation processes; however, a larger effect is recorded for TLS-separated cells.

2) Edge Passivation Stability: Based on the *pFF* results, the passivation stability investigation (see Fig. 10) shows that the cells coated with $d_2 = 14$ nm remain almost constant with minimal ($\Delta pFF \approx 0.1\%_{\mathrm{abs}}$) to no measured decrease. These results show a stable edge passivation over time for the cells coated with $d_2 = 14$ nm AlO_X, while cells with $d_1 = 7$ nm or without degrade with time. The explanation for the time-based passivation stability on the deposited layer thickness is under further investigation.

C. IV Measurement Results

Based on the results of the previous section, the favored processes for the fabrication of edge-passivated cells are used to fabricate cells for IV measurements. Host wafers are separated into shingle cells by means of TLS. The cells are then coated using an identical thermal ALD deposition process to the one used before. This time this leads to around 13-nm-thick postmetallization AlO_X layer. The cells are then annealed on a hotplate.

IV measurements of TLS-separated edge-passivated pSPEER$^{\mathrm{PET}}$ solar cells are done in comparison to LSMC-separated pSPEER solar cells that do not undergo any further processes after separation. The front- and rear-side IV measurement data from the most efficient cells are summarized

TABLE I
IV MEASUREMENT DATA FOR THE CELLS WITH HIGHEST OUTPUT POWER DENSITIES FOR TLS+PET-PROCESSED AND LSMC-SEPARATED CELLS IN ADDITION TO AVERAGE VALUES OF THE FRONT-SIDE MEASUREMENTS

Meas. side	η (%)	V_{OC} (mV)	$j_{SC,des}$ (mA/cm^2)	FF (%)	pFF (%)	r_S (Ω cm^2)	β (%)	p_{out} (mW/cm^2)
TLS separated pSPEER^{PET} solar cell								
Front Av.	21.8	668	40.4	81.0	82.6	0.38	-	
Front Peak	22.1	669	40.5	81.4	83.2	0.38	67	23.5
Rear Peak	14.7	660	27.2	81.8	82.8	0.35		
LSMC separated pSPEER solar cell								
Front Av.	21.6	664	40.2	81.0	82.3	0.35	-	
Front Peak	21.7	667	40.3	80.9	82.4	0.35	66	23.1
Rear Peak	14.4	657	27.0	81.0	82.0	0.35		

Characteristic data for the front- and rear-side measurements are shown. Front- and rear-side measurements are separately performed at $G = 1000$ W/m^2. Since the busbar is intended to be covered in the module, a designated area $j_{SC,des}$ excluding the busbar area is considered. p_{out} considers an additional 10% irradiance from the rear side.

in Table I. For the front-side measurements, average values (Av.) are also shown. The TLS-separated cell after PET treatment yields a designated front-side energy conversion efficiency $\eta_f = 22.1\%$, featuring $V_{OC} = 669$ mV, $FF = 81.4\%$, and short-circuit current density $j_{SC,des} = 40.5$ mA/cm^2. Due to the PET treatment, the cell features a high $pFF = 83.2\%$. Even though PET is included as postfiring thermal process, a low $r_S = 0.38\ \Omega$ cm^2 is achieved, hinting that no significant degradation at the metal contacts occurs. The LSMC-separated cell without PET attains $\eta_f = 21.7\%$. In comparison to the pSPEER cell, the pSPEER^{PET} cell features a higher front-side efficiency $\Delta\eta_f = +0.4\%_{abs}$, which can be attributed to the higher short-circuit current density $\Delta j_{SC} = +0.2$ mA/cm^2 and $\Delta FF = +0.5\%_{abs}$. This difference in FF can be explained by the higher pFF of $+0.8\%_{abs}$, while featuring a slightly higher r_S.

Mainly, the improved pFF is a result of an enhanced edge quality obtained by the TLS process and the additional PET processes.

The rear-side measurement results also show similar trends, where the pSPEER^{PET} cell attains a designated rear-side energy conversion efficiency $\eta_r = 14.7\%$ that is $+0.3\%_{abs}$ higher than the LSMC-separated pSPEER cell that attains $\eta_r = 14.4\%$. The difference in $\Delta pFF = +0.8\%_{abs}$ is entirely projected on the $\Delta FF = +0.8\%_{abs}$ due to the identical rear side $r_S = 0.35\ \Omega$ cm^2 between the two compared cells. The TLS-separated and edge-passivated solar cell attains a bifaciality $\beta = \eta_r/\eta_f = 0.67$, whereas the LSMC-separated cell without PET attains $\beta = 0.66$.

Considering an additional 10% rear-side irradiance $G_r = 100$ W/m^2, the edge-passivated cell attains an output power density $p_{out} = 23.5$ mW/cm^2. This value is greater by $\Delta p_{out} = +0.4$ mW/cm^2 in comparison to the nonpassivated LSMC-separated cell.

The result of the TLS + PET processed cell shows its clear advantage in terms of efficiency. Therefore, we have demonstrated the functionality of the proposed PET postmetallization edge passivation approach. No changes in the premetallization processes in an industrial production line are required. The integration of PET into the fabrication after the separation of silicon solar cells (i.e. shingle cells, half-cut cells, or small-area cells) can, thus, lead to a significant boost in cell efficiency with a relatively reasonable integration within the already existing production infrastructure. This makes the proposed PET attractive for industrial application and incorporation in production lines.

V. CONCLUSION

This article introduces a postmetallization/separation PET for separated solar cells. The effect of PET on bifacial p-type silicon shingled passivated edge, emitter, and rear solar cells (pSPEER) is tested. After edge passivation, we call the PET-treated shingle cells "pSPEER^{PET}" solar cells.

The TLS process leaves the separated cells with visibly smoother edges in comparison to separation by LSMC. By just considering the separation processes without further PET, the separation processes lead to similar drops in pseudo fill factor pFF of $\Delta pFF \approx -1.2\%_{abs}$.

For the PET deposition process, low-temperature thermal ALD of AlO_X for two layer thicknesses $d_1 = 7$ nm and $d_2 = 14$ nm is performed. TLS-separated PET-treated pSPEER^{PET} cells have regained half the loss that is induced due to separation. The pFF increase from as-separated TLS-cut cells to edge-passivated cells is found to be up to $+0.7\%_{abs}$, while LSMC-separated cells gain up to $+0.3\%_{abs}$ after PET. Thereby, the cells with $d_2 = 14$-nm-thick AlO_X layer show constant pFF values within the experimental time frame of 167 h after passivation, thus indicating the stability of the passivation.

After TLS and PET, the best pSPEER^{PET} solar cell attains a designated front-side energy conversion efficiency $\eta_f = 22.1\%$. Assuming an additional rear-side irradiance $G_r = 100$ W/m^2, this cell features a total output power density $p_{out} = 23.5$ mW/cm^2. TLS followed by PET leads to a higher output power density of $\Delta p_{out} = +0.4$ mW/cm² compared to a PET-free LSMC-separated cell. The PET treatment introduced in this article shows a clear benefit and the thus processed and separated solar cells achieve higher p_{out} values.

The proposed PET is a promising postmetallization edge passivation treatment that might be realized in the industry without requiring adjustments in premetallization stages.

ACKNOWLEDGMENT

The authors would like to thank C. Schmiga for SEM images. The authors would also like to thank B. Bläsi for the module reflection simulations. Special thanks to Fraunhofer ISE Photovoltaics Division colleagues. This work was supported by the German Federal Ministry for Economic Affairs and Energy within the research project "PV-BAT400" under Contract 0324145.

REFERENCES

[1] J. D. C. Dickson, "Photo-voltaic semiconductor apparatus or the like," US Patent 2 938 938, May 31, 1960.

[2] R. J. Nielsen and R. Leif, "Satellite solar cell assembly," US Patents 3 116 171A, 3 116 171, Dec. 31, 1963.

[3] S. W. Glunz *et al.*, "High-efficiency silicon solar cells for low-illumination applications," in *Proc. 29th IEEE Photovolt. Specialists Conf.*, New Orleans, LO, USA, 2002, pp. 450–453.

[4] J. Zhao, A. Wang, D. M. Roche, S. R. Wenham, and M. A. Green, "Pilot production of high efficiency PERL silicon solar cells for the world solar challenge solar car race," in *Proc. 29th IEEE Photovolt. Specialists Conf.*, New Orleans, LO, USA, 2002, pp. 65–66.

[5] D. Tonini, M. Bertazzo, A. Fecchio, and M. Galiazzo, "Shingling technology for cell interconnection: Technological aspects and process integration," in *Proc. 33rd Eur. PV Solar Energy Conf. Exhib.*, Amsterdam, The Netherlands, 2017.

[6] H. Schulte-Huxel, S. Blankemeyer, A. Morlier, R. Brendel, and M. Köntges, "Interconnect-shingling: Maximizing the active module area with conventional module processes," *Solar Energy Mater. Solar Cells*, vol. 200, 2019, Art. no. 109991.

[7] D. Rudolph *et al.*, "Cell design optimization for shingled modules," in *Proc. 33rd Eur. PV Solar Energy Conf. Exhib.*, Amsterdam, The Netherlands.

[8] P. Papet *et al.*, "Overlap modules: A unique cell layup using Smart Wire Connection Technology," in *Proc. AIP Conf.*, 2019, vol. 2147, pp. 080001-1–080001-5.

[9] E. Sung and J. Zu-Li Liu, "Systems, method and apparatus for curing," US Patent 9 748 434B1, Aug. 29, 2017.

[10] R. Morad *et al.*, "Shingled solar cell module," US Patent 9397252 B2 US 14/594,439, Jul. 19, 2016.

[11] R. Morad *et al.*, "Shingled solar cell module," US Patent 2015/0349167 A1.

[12] *SunPower Corporation SunPower Introduces New Solar Panel: The Performance Series*. Available: https://us.sunpower.com/solar-panelstechnology/ p-series-solar-panels/

[13] CanadianSolar Inc, "High density shingle modules." [Online]. Available: https://canadiansolar.com/solarPanels/detail/28

[14] J. Schneider, S. Schoenfelder, S. Dietrich, and M. Turek, "Solar module with half size solar cells," in *Proc. 29th Eur. PV Solar Energy Conf. Exhib.*, Amsterdam, The Netherlands, pp. 185–189,2014.

[15] M. Hermle, J. Dicker, W. Warta, S.W. Glunz, and G. Willeke, "Analysis of edge recombination for high-efficiency solar cells at low illumination densities," in *Proc. 3rd World Conf. Photovolt. Energy Convers.*, 2003, pp. 1009–1012.

[16] J. Dicker, "Analyse und Simulation von hocheffizienten Silizium-Solarzellenstrukturen für industrielle Fertigungstechniken," Dissertation, Fakultät für Physik, Universität Konsatnz, 2003.

[17] K. Ruhle, M. K. Juhl, M. D. Abbott, L. M. Reindl, and M. Kasemann, "Impact of edge recombination in small-area solar cells with emitter windows," *IEEE J. Photovolt.*, vol. 5, no. 4, pp. 1067–1073, Jul. 2015.

[18] J. Zhao, A. Wang, P. P. Altermatt, and G. Zhang, "Peripheral loss reduction of high efficiency silicon solar cells by MOS gate passivation, by poly-Si filled grooves and by cell pattern design," *Prog. Photovolt. Res. Appl.*, vol. 8, no. 2, pp. 201–210, 2000.

[19] W. P. Mulligan, A. Terao, D. D. Smith, P. J. Verlinden, and R. M. Swanson, "Development of chip-size silicon solar cells," in *Proc. 28th IEEE Photovolt. Specialists Conf. Record*, Anchorage Hilton Hotel, Anchorage, AK, USA, Sep. 15–22, 2000, pp. 158–163.

[20] P. P. Altermatt, G. Heiser, and M. A. Green, "Numerical quantification and minimization of perimeter losses in high-efficiency silicon solar cells," *Prog. Photovolt. Res. Appl.*, vol. 4, no. 5, pp. 355–367, 1996.

[21] S. Schäfer *et al.*, "26%-efficient and 2 cm narrow interdigitated back contact silicon solar cells with passivated slits on two edges," *Sol. Energy Mater. Sol. Cells*, vol. 200, Sep. 2019.

[22] T. Fellmeth, "Silicon solar cells for the application in low concentrator systems—Development and characterization," Dissertation der Mathematisch-Naturwissenschaftlichen Fakultät, Universität Tübingen, 2014, pp. 35–37.

[23] N. Wöhrle *et al.*, "The SPEER solar cell simulation study of shingled bifacial PERC technology based stripe cells," in *Proc. 33rd Eur. PV Solar Energy Conf. Exhib.*, Amsterdam, The Netherlands, 2017, pp. 844–848.

[24] N. Wöhrle *et al.*, "Solar cell demand for bifacial and singulated-cell module architectures," *Photovolt. Int.*, vol. 36, no. 36, pp. 48–62, 2017.

[25] P. Baliozian *et al.*, "Bifacial p-type silicon shingle solar cells – The "pSPEER" concept," *Sol. RRL*, vol. 2, no. 3, 2018, Art. no. 1700171.

[26] A. W. Blakers, A. Wang, A. M. Milne, J. Zhao, and M. A. Green, "22.8% efficient silicon solar cell," *Appl. Phys. Lett.*, vol. 55, no. 13, pp. 1363–1365, 1989.

[27] H. U. Zuehlke, G. Eberhardt, and P. Mende, "TLS-Dicing – the way to higher yield and throughput," in *Proc. Int. Symp. Semicond. Manufactur.*, 2008, vol. 2008, no. 17, pp. 301–304.

[28] D. Lewke, "Untersuchung und Minimierung Lateraler Rissabweichungen beim Thermischen Laserstrahlseparieren," Dissertation, von der Technischen Fakultät der Friedrich-Alexander, Universität Erlangen-Nürenberg, 2017.

[29] B. Hoex, S. S. S. Heil, E. Langereis, M. C. M. Van de Sanden, and W. M. M. Kessels, "Ultralow surface recombination of c-Si substrates passivated by plasma-assisted atomic layer deposited Al_2O_3," *Appl. Phys. Lett.*, vol. 89, p. 1, 2006.

[30] A. Richter, J. Benick, M. Hermle, and S. W. Glunz, "Excellent silicon surface passivation with 5 Å thin ALD Al_2O_3 layers: Influence of different thermal post-deposition treatments," *Phys. Status Solidi RRL*, vol. 5, no. 5–6, pp. 202–204, 2011.

[31] A. Richter, Aluminum oxide for the surface passivation of high efficiency silicon solar cells: Technology and advanced characterization. Ph.D. dissertation, Zugl., Konstanz, Univ., Stuttgart, Germany: Fraunhofer-Verlag, 2015.

[32] A. Richter, J. Benick, A. Kimmerle, M. Hermle, and S. W. Glunz, "Passivation of phosphorus diffused silicon surfaces with Al_2O_3: Influence of surface doping concentration and thermal activation treatments," *J. Appl. Phys.*, vol. 116, no. 24, 2014, 243501.

[33] C. Chan *et al.*, "Instabilitiy of increased contact resistance in silicon solar cells following post-firing thermal processes," *Sol. RRL*, vol. 2017, no. 1, Art. no. 1700129(1–5).

[34] 3D-Micromac AG, Microdice – TLS-Dicing^{TM} System zum Separieren von Silizium- und Siliziumkarbid-Wafern. [Online]. Available: https://3d-micromac.de/laser-mikrobearbeitung/produkte/microdice/. Accessed: Aug. 30, 2019.

[35] P. Baliozian, T. Fellmeth, N. Wöhrle, E. Lohmüller, and R. Preu, "Bifacial pSPEER solar cells for shingle modules," in *Proc. 35th Eur. PV Solar Energy Conf. Exhib.*, Brussels, Belgium, pp. 410–413, 2018.

[36] R. A. Sinton, "Possibilities for process-control monitoring of electronic material properties during solar-cell manufacture," *Proc. 9th Workshop Crystalline Silicon Sol. Cell Mater. Processes*, Colorado, USA, 1999, pp. 67–73.

[37] D. Bertrand, S. Manuel, M. Pirot, A. Kaminski-Cachopo, and Y. Veschetti, "Modeling of edge losses in Al-BSF silicon solar cells," *IEEE J. Photovolt.*, vol. 7, no. 1, pp. 78–84, Jan. 2017.

[38] S. I. Raider, R. Flitsch, and M. J. Palmer, "Oxide growth on etched silicon in air at room temperature," *J. Electrochem. Soc.*, vol. 122, no. 3, pp. 413–418, 1975.

[39] Oxford Instruments, FlexAL. Available: https://plasma.oxinst.com/products/ald/flexal

[40] R. A. Sinton, A. Cuevas, and M. Stuckings, "Quasi-steady-state photoconductance, a new method for solar cell material and device characterization," in *Proc. 25th IEEE Photovolt. Specialists Conf.*, 1996, vol. 1996, pp. 457–460.

[41] A. B. Sproul, "Dimensionless solution of the equation describing the effect of surface recombination on carrier decay in semiconductors," *J. Appl. Phys.*, vol. 76, no. 5, pp. 2851–2854, 1994.

[42] A. Fell *et al.*, "Modeling edge recombination in silicon solar cells," *IEEE J. Photovolt.*, vol. 8, no. 2, pp. 428–434, Mar. 2018.

Puzant Baliozian was born in Beirut, Lebanon, in 1993. He received the B.Sc. degree in physics from the American University of Beirut, in 2014, and the M.Sc. degree in renewable energy engineering and management from the University of Freiburg, Freiburg im Breisgau, Germany, for his thesis work completed at Fraunhofer IPM in the field of magnetocaloric energy conversion, in 2016. He is currently working toward the Ph.D. degree at Fraunhofer ISE, Freiburg im Breisgau.

His main research interests include development of *p*-type SPEER solar cells by focusing on the laser-assisted separation and edge passivation processes.

Mohammad Al-Akash was born in Amman, Jordan, in 1993. He received the B.Sc. degree in energy engineering from German Jordanian University, Madaba, Jordan. He received the M.Sc. degree in renewable energy engineering and management from the University of Freiburg, Freiburg im Breisgau, Germany, in 2019. His master thesis done at Fraunhofer ISE focused on the evaluation of different postmetallization edge passivation methods of *p*-type SPEER solar cells.

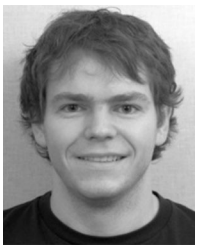

Elmar Lohmüller was born in Tübingen, Germany, in 1983. He received the graduation in physics from the University of Tübingen, Tübingen, Germany, and Nelson Mandela Metropolitan University, Port Elizabeth, South Africa. He received the Ph.D. degree from the University of Freiburg, Freiburg im Breisgau, Germany, in 2015, for his work on the development of *n*-type MWT solar cells.

He is currently a Researcher, Project and Product Manager with the Fraunhofer ISE. His research interests include development of *p*-type PERC solar cells.

Armin Richter received the Ph.D. degree in physics from the University of Konstanz, Germany, in 2014, for the work on *n*-type silicon solar cells with front-side boron-doped emitters and the in-depth characterization of aluminum oxide-based silicon surface passivation.

His current research interests include atomic layer deposition of functional thin films (e.g., passivation layers, electron/hole transport layers, TCOs), in-depth characterization of dielectric surface passivation layers, as well as the development of high-efficiency silicon solar cells along the whole process chain and 3-D device simulations.

Tobias Fellmeth received the graduation degree in physics from the University of Konstanz, Konstanz, Germany, for his work on the development and characterization of MWT concentrator solar cells. He received the Ph.D. degree from the University of Tübingen, Tübingen, Germany, in 2014, for his work on silicon-based, low concentrator solar cells.

He is currently a Scientist and Project Manager with the Fraunhofer ISE, Freiburg im Breisgau. His research interests include development of bi-facial PERC and TOPCon solar cells.

Anna Münzer was born in Stuttgart, Germany, in 1991. She received the B.Sc. degree in physics from the University of Tübingen, Tübingen, Germany, with a focus on semiconductor physics, in 2015. Afterwards, she studied renewable energy engineering and management at the University of Freiburg.

Since 2018, she has been an Engineer with the Fraunhofer ISE, Freiburg im Breisgau, where she is currently working on TLS process development in the research on shingled solar cells.

Nico Wöhrle was born in Breisach, Germany, in 1984. He received the graduation degree in physics from the University of Freiburg, Freiburg im Breisgau, Germany, for his work on optical simulation of silicon solar cells, in 2012. With a fellowship from the German Federal Environmental Foundation (DBU), he received the Ph.D. degree from the University of Freiburg, in 2016, for his work on simulation of PERC solar cells.

He is currently a Researcher with the Fraunhofer ISE, Freiburg im Breisgau. His research interests include simulation and inline characterization of solar cells as well as the conceptual development of *p*-type PERC solar cells.

Pierre Saint-Cast was born in Lorient, France, in 1982. He received the M.Sc. and Engineering degrees from the Polytechnic Institute of Grenoble, Grenoble, France, in 2007, and the Ph.D. degree from the University of Konstanz, Germany, in 2012.

Since 2008, he has been with the Fraunhofer Institute for Solar Energy Systems (ISE), Freiburg, Germany. He is currently the Project Manager and Product Manager for PERC solar cells at the Fraunhofer ISE, Freiburg im Breisgau, Germany. His research interests include the development of passivation layers for solar cell applications, especially plasma-enhanced chemical vapor deposition of Al_2O_3 layers, and the analytical modeling of electrical transport in Si solar cells devices.

Hannah Stolzenburg was born in 1993. She received the graduation degree in physics from the University of Göttingen, Germany. She received the M.Sc. degree in 2018 with the focus on material and solid-state physics while spending one semester studying physics at the University of Ghent. Currently, she is working toward the Ph.D. degree, on characterization and quantification of edge losses in silicon solar cells, with the Fraunhofer ISE, Freiburg im Breisgau, Germany.

Alma Spribille received the Diploma in energy and environmental management from the Europe-University of Flensburg, Flensburg, Germany.

She wrote her diploma thesis as an Industrial Engineer at Fraunhofer ISE about MWT solar cells in 2010 and joined the group MWT Solar Cells & Printing Technology.

Since December 2017, she has been heading the team process integration – structuring and metallization.

Ralf Preu was born in Stuttgart, Germany, in 1967. He received the graduation degree in physics from the Universities of Freiburg, Germany and the degree in economics from the University of Hagen, Germany. He received the Ph.D. degree in electrical engineering.

He is currently the Director of the Division for PV Production Technology, Fraunhofer Institute for Solar Energy Systems (ISE), Freiburg, Germany. He joined Fraunhofer ISE in 1993 and has worked in different fields in PV, including system monitoring, silicon solar cell and module technology, characterization and simulation. He teaches photovoltaics at the University of Freiburg, Freiburg im Breisgau, Germany. His research interests include development of advanced silicon solar cell technology and its transfer to industrial production.